Geophysical Research Letters

RESEARCH LETTER
10.1029/2019GL082488

Initial Breakdown Pulses Accompanied by VHF Pulses During Negative Cloud-to-Ground Lightning Flashes

Ivana Kolmasova[1,2], Thomas Marshall[3], Sampath Bandara[3], Sumedhe Karunarathne[4], Maribeth Stolzenburg[3], Nilmini Karunarathne[3], and Raymond Siedlecki[3]

[1]Department of Space Physics, Institute of Atmospheric Physics AS CR, Prague, Czechia, [2]Faculty of Mathematics and Physics, Charles University, Prague, Czechia, [3]Physics and Astronomy, University of Mississippi, Oxford, MS, USA, [4]Physics Department, Baptist College of Health Sciences, Memphis, TN, USA

Key Points:
- In cloud-to-ground lightning, classical initial breakdown pulses are systematically accompanied by very high frequency radiation
- The relative amplitudes of the coincident low and very high frequency pulses are variable and weakly correlated or uncorrelated
- Initial lightning extensions occur as a fast and variable process on multiple length scales inside a thundercloud

Supporting Information:
- Supporting Information S1
- Data Set S1
- Data Set S2
- Data Set S3
- Data Set S4
- Data Set S5
- Data Set S6
- Data Set S7
- Data Set S8
- Data Set S9

Correspondence to:
I. Kolmasova,
iko@ufa.cas.cz

Citation:
Kolmasova, I., Marshall, T., Bandara, S., Karunarathne, S., Stolzenburg, M., Karunarathne, N., & Siedlecki, R. (2019). Initial breakdown pulses accompanied by VHF pulses during negative cloud-to-ground lightning flashes. *Geophysical Research Letters*, *46*, 5592–5600. https://doi.org/10.1029/2019GL082488

Received 16 FEB 2019
Accepted 2 MAY 2019
Accepted article online 8 MAY 2019
Published online 25 MAY 2019

Abstract This study compares waveforms recorded by "broadband" very low frequency/low-frequency/medium-frequency (VLF/LF/MF) electric field change sensors (bandwidth ~0–2.5 MHz) and very high frequency (VHF) sensors (bandwidth 186–192 MHz) during the initiation of 20 negative cloud-to-ground lightning flashes. In the first 2 ms of each flash, initial breakdown (IB) pulses are detected with the VLF/LF/MF sensors. Comparison shows that all classical IB pulses are accompanied by VHF pulses, where classical IB pulses are defined herein as bipolar with duration >10 μs and amplitude >25% of the largest IB pulse amplitude in the flash. There are on average 47% of IB pulses (of all amplitudes and durations) that are accompanied by VHF pulses within ±1 μs. There are also many VHF pulses with no associated IB pulses. These observations indicate that the initial in-cloud lightning channel extension process (es) occurs very fast and at multiple length scales, since substantial electromagnetic radiation is emitted in the VLF/LF/MF and VHF bands.

Plain Language Summary There is a lack of understanding of how a lightning flash initiates, as this process usually takes place deep inside thunderclouds. Electromagnetic pulses emitted during lightning initiation, which can be measured from a safe distance, help us to understand lightning better. We use arrays of low-frequency (~0–2.5 MHz) and very high frequency (186–192 MHz) receivers and compare their recordings registered during initiation of 20 cloud-to-ground lightning flashes. We found that the larger pulses detected during lightning initiation in low-frequency records were systematically accompanied by pulses detected in the very high frequency records. This observation indicates that the initial lightning extension process occurs very fast and at multiple length scales and that emitted electromagnetic radiation covers a very large range of frequencies.

1. Introduction

Cloud-to-ground (CG) lightning flashes typically begin with an initiating event and an IEC (defined below and lasting 0.1–0.3 ms), followed by a sequence of initial breakdown (IB) pulses, followed by a stepped leader that results in the first return stroke (RS) of the flash (e. g., Marshall, Schulz, et al., 2014; Marshall, Stolzenburg, et al., 2014). IB pulses, which are the focus of this study, are often detected with electric field change (E-change) sensors operating in the low-frequency (LF) radio band or with broadband (very low frequency/LF/medium-frequency) E-change sensors (e.g., Weidman & Krider, 1979). As defined herein, IB pulses are mainly *bipolar* pulses of varying amplitudes, with durations of roughly 1–80 μs for CG flashes, though unipolar pulses are occasionally found (Stolzenburg et al., 2013; Weidman & Krider, 1979). For convenience in this work, we define below several types of IB pulses. The initial polarity of IB pulses is usually identical to the polarity of the following first RS during a negative CG flash (Baharudin et al., 2012; Weidman & Krider, 1979). The amplitudes of the largest IB pulses are mostly smaller than the amplitudes of the following RS pulse; exceptionally, they were observed to be comparable to the RS pulse peak amplitudes (Brook, 1992; Baharudin et al., 2012; Marshall, Schulz, et al., 2014). In CG flashes the sequence of IB pulses lasts for 2–10 ms (Clarence & Malan, 1957); herein, we focus on the first 2 ms only. The time interval between the first IB pulse and the corresponding first RS (IB-RS) is usually several tens of milliseconds (Marshall, Schulz, et al., 2014); nevertheless IB-RS time intervals as short as a few of milliseconds were also reported for winter or winter-like thunderstorms (Brook, 1992; Kolmašová et al., 2014; Wu et al., 2013). IB pulses are thought to be generated by currents flowing in the intermittently extending in-cloud lightning leaders

(Stolzenburg et al., 2013). The IB pulses can be detected hundreds of kilometers from the parent thunderstorm (Kolmašová et al., 2016; Kotovsky et al., 2016) and are one indication of lightning initiation. Another indication of lightning initiation is an initial E-change (IEC) that occurs immediately before the first IB pulse and can be detected only at short distances (typically within 7 km) from the developing discharge (Chapman et al., 2017; Marshall, Stolzenburg, et al., 2014; Marshall et al., 2019). Based on very high frequency (VHF) interferometric measurements, Rison et al. (2016) hypothesized that many or all lightning flashes are initiated by a phenomenon called fast positive breakdown, which they explained as a system of positive streamers developing in a locally intense electric field region. Marshall et al. (2019) found that for two CG lightning flashes, IECs were accompanied by VHF pulses measured by an array of "LogRF" receivers working in a frequency band of 6 MHz centered at 189 MHz. They speculated that the LogRF events were positive corona streamers needed for the following negative breakdown of the IB pulses.

Properties of IB pulses have been intensively studied by different groups of researchers (Baharudin et al., 2012; Karunarathne et al., 2013; Kolmašová et al., 2014, 2016; Marshall, Schulz, et al., 2014, Marshall, Stolzenburg, et al., 2014; Stolzenburg et al., 2014; Wu et al., 2013). IB pulses were found to be clearly accompanied by luminosity changes (Stolzenburg et al., 2013; Wilkes et al., 2016). A possible correspondence of IB pulses and terrestrial gamma ray flashes was also reported (Cummer et al., 2015; Lu et al., 2010; Marshall et al., 2013, 2017). Nevertheless, a correspondence of sources of impulsive VHF radiation detected by LMA (Lightning Mapping Array) systems with IB pulses seemed to be absent or very weak (Hare et al., 2017; Wilkes et al., 2016). A recent detailed analysis (Kolmašová et al., 2018) discovered that individual peaks of strong VHF radiation seen by separate LMA stations corresponded surprisingly well to the IB pulses. The analysis was limited by the performance of LMA stations that reported only the strongest VHF source within each 80-μs-long LMA window.

In this study, we benefit from simultaneous measurements from arrays of VHF sensors (Marshall et al., 2019) and broadband E-change sensors (Karunarathne et al., 2013). We focus on comparisons of waveforms recorded during the first 2 ms of the initiation of 20 negative CG lightning flashes. We use data collected during two thunderstorms that occurred in August 2016. In section 2 we introduce our instrumentation, and in section 3 we describe the data set. In section 4 we analyze recorded waveforms. In section 5 we discuss the results.

2. Instrumentation

The array of sensors was deployed at seven sensor sites within 45 km of Oxford, Mississippi, USA; a map of the seven stations is shown in Figure 2c in Marshall et al. (2019). For this study, we use the data from two stations called EE and FS. Four types of sensors were placed at each sensor site. These sensors are called Slow Antenna (SA), Fast Antenna (FA), dE/dt, and LogRF sensors. The FA and SA sensors are calibrated E-change sensors with 1-s and 10-ms electronic decay times, respectively, and bandwidths of 0.16 Hz to 2.6 MHz and 16 Hz to 2.6 MHz, respectively. Detailed description of the sensors can be found in Marshall et al. (2019). For this study we are using the SA data recorded continuously at a sampling rate of 10 kHz to identify the lightning flashes. For the detailed analysis we are using the triggered FA data and LogRF data both sampled at 10 MS/s. The FA data show the IB pulses, while the LogRF sensors show the VHF pulses. The FA data are averaged to 5 MS/s. The pretrigger time was set to 250 ms. The total length of each waveform record was set to 400 ms. The LogRF sensors are logarithmic amplifiers with a dynamic range of 55 dBm detecting the received power of signals in a frequency band of 6 MHz centered at 189 MHz. To capture a LogRF record of data, a trigger from the FA was used. Each sensor site is equipped with a GPS receiver to time-tag digitized signals.

3. Data Set

We have chosen two thunderstorms that occurred during the 2016 campaign (5 and 25 August 2016) for our analysis. The FA data from these thunderstorms were visually inspected in order to select 20 flashes, which met predefined criteria and are still sufficiently different in order to perform a reliable analysis. Used criteria are as follows: (a) The sequence of IB pulses occurred at the beginning of a negative CG flash. (b) The sequence of IB pulses lasted at least 3 ms. (c) Larger IB pulses occurred only within the first 2 ms of the flash. (d) The developing in-cloud discharge was propagating generally downward based on the Position By Fast

Antenna geolocation method for IB pulses (Karunarathne et al., 2013). (e) Except for initiation activity (e.g., the initiating event and IEC) in the millisecond immediately preceding the first IB pulse, we required that there was an electrically quiet period of many milliseconds before the first IB pulse in each flash (Chapman et al., 2017; Marshall, Stolzenburg, et al., 2014; Marshall et al., 2019). Starting with the first IB pulse, we investigated 2-ms durations of FA and LogRF recordings in detail for all 20 selected flashes.

4. Analysis of Waveforms

4.1. Comparison of FA and LogRF Waveforms

For the comparison of FA and LogRF waveforms we used data recorded at the EE or FS station, whichever was closer to the developing discharge. We have used EE station data in 16 flashes and FS station data in the remaining 4 flashes. Two examples of FA and LogRF waveforms recorded at EE station are shown in Figure 1. Each example displays 2.5 ms of data. Waveforms in Figures 1a and 1b were captured on 5 August 2016, and waveforms in Figures 1d and 1e were recorded on 25 August 2016. Figures 1a and 1d show the waveforms measured by the LogRF receiver, Figures 1b and 1e represent the waveforms recorded by the broadband FA receiver. Red dots plotted in Figures 1b, 1c, 1e, and 1f are the occurrence heights of individual IB pulses estimated using the Position By Fast Antenna method (Karunarathne et al., 2013). The dotted red lines in Figures 1c and 1f representing linear fits confirm the downward propagation of developing in-cloud discharges. The 2.0 ms of data investigated in detail starts at the time of occurrence of the first IB pulse in the FA records and is indicated by vertical blue arrows in Figures 1b and 1e.

We have estimated a noise level in each record in order to include in our data set all IB pulses (in the FA data) with amplitudes exceeding twice this estimated noise level, which is 166 mV/m for the data in Figure 1b and 139 mV/m for the data in Figure 1e (and varies from 83 to 245 mV/m for the other 18 flashes studied). We identified "classical" IB pulses in our FA records based on the following characteristics (e.g., Nag et al., 2009; Weidman & Krider, 1979): amplitude exceeding 25% of the amplitude of the largest IB pulse, bipolar pulse shape, often having subpulses, and duration exceeding 10 μs. Herein, we call bipolar or unipolar IB pulses with durations shorter than 10-μs "narrow IB pulses." Narrow IB pulses tend to have amplitudes <25% of the amplitude of the largest IB pulse. Note that for each CG flash our resulting data set of FA pulses includes classical IB pulses, narrow IB pulses, smaller amplitude bipolar pulses and unipolar pulses with durations >10 μs, and unipolar subpulses occurring on leading or trailing edges of classical IB pulses.

Separately, we also constructed a data set of VHF pulses in the LogRF records with relative amplitudes exceeding 3 times the impulsive background noise. As this impulsive noise was unfortunately superposed on a slowly varying background of unknown origin we decided to subtract this slowly varying component from the VHF peak amplitudes and to use these relative amplitudes. Larger subpulses were considered as separate VHF pulses. The level of the impulsive background noise was estimated in the range of 10–60 mV for different records, which corresponds to a received VHF power of −76.0 to −74.0 dBm. A typical value of the smallest VHF power of pulses included in our analysis is −74.5 dBm.

Among the 20 CG flashes we found that the IB pulse with the largest amplitude occurred on average 0.5 ms after the first recognizable IB pulse; this value is in good agreement with an average of 0.6 ms for 32 CG flashes in Florida determined by Smith et al. (2018). In these same flashes the most energetic VHF pulse was found on average 1 ms after the first recognizable IB pulse. The time differences between the largest IB pulses and the most energetic VHF pulses varied from −0.7 to 1.8 ms in our data set. Note that since the VHF relative amplitudes were estimated manually using a local background level, it may seem as if the largest VHF pulse chosen was smaller than another VHF pulse in Figures 1a and 1d (see their times in Table 1). However, the explanation is that the VHF data in Figures 1a and 1d include the slowly varying background that is subtracted before determining the largest VHF pulse amplitude, as shown in supporting information Figures S3 and S4.

4.2. Correspondence of Classical IB Pulses and VHF Pulses

Taking into account the results of Marshall et al. (2019), who studied the first one or two classical IB pulses in two CG flashes and two intra-cloud (IC) flashes and found significant VHF pulses occurring within the duration of each IB pulse, and findings of Kolmašová et al. (2018) who report that larger magnetic field IB pulses

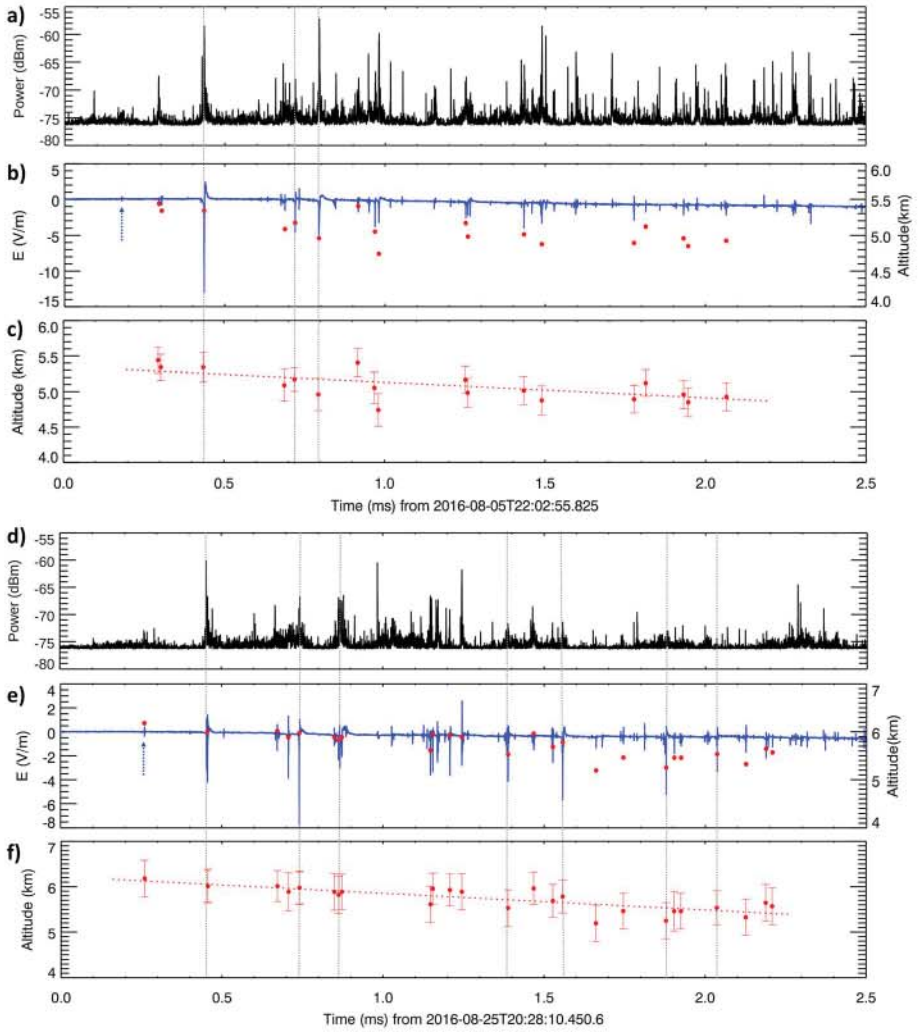

Figure 1. Examples of Fast Antenna and LogRF data recorded at the EE station on 5 August 2016 (a–c) and on 25 August 2016 (d–f). Black curves represent the calibrated waveforms measured by the LogRF receiver, and blue curves represent the calibrated waveforms recorded by the broadband E-change receiver. Blue arrows indicate the time of occurrence of the first recognizable pulse in Fast Antenna records used as a start of the investigated 2-ms-long waveform capture. Red dots plotted in panels (b), (c), (e), and (f) point at the occurrence heights of individual initial breakdown pulses calculated using the Position By Fast Antenna method. Vertical grey dotted lines identify very high frequency pulses occurring within durations of classical initial breakdown pulses. Dotted red lines in panels (c) and (f) represent linear trends indicating the downward propagation of developing discharge.

were systematically accompanied by VHF pulses in raw LMA (VHF) records, we first look for an occurrence of VHF pulses anytime within the duration of classical IB pulses. To be able to identify classical IB pulses, we downsampled the FA waveforms to 1 MHz to get rid of narrower pulses and subpulses. Then for each IB pulse, the duration of the pulse was calculated as a time difference between the time when the pulse amplitude exceeds 10% of its peak value and the time when it returns back to 10% of the opposite polarity overshoot value. The resulting data set consists of 201 classical IB pulses in the FA data for 20 CG flashes. The mean duration of classical IB pulses found within individual sequences varies from 16 to 34 μs, and the duration of the longest pulse in the whole data set is 65 μs.

Next we checked for the presence of a VHF pulse (above the noise level) occurring within the whole duration of each classical IB pulse. Among these 201 events, *we find that VHF pulses systematically accompany all classical IB pulses*. All pairs of classical IB pulses and accompanying VHF pulses identified in examined pairs of waveforms in Figure 1 are shown by vertical gray dashed lines. In some cases, the peaks of the VHF power were not precisely coincident in time with classical IB pulse peaks; for example, some VHF peaks appeared

Geophysical Research Letters

10.1029/2019GL082488

Table 1
IB Pulses and IB-VHF Pairs Occurring During the First 2 ms of a Flash Development

1	2	3	4	5	6	7	8	9	10	11	12
5 August 2016	Number of all IB pulses (number of l arge IB pulses)	Number of classical IB pulses	Mean duration of classical IB pulses (μs)	Mean power of VHF radiation sources (W)	Number of IB-VHF pairs in 2 ms	Portion of IB with VHF in ±1 μs (%)	Portion of large IB-VHF pairs (%)	Portion of small IB-VHF pairs (%)	Portion of VHF with IB in ± 1 μs (%)	Position of IB_{max} (ms)	Position of VHF_{max} (ms)
1	110 (17)	13	26.3	10.8	62	56	76	53	26	0.57	1.31
2	35 (19)	10	19.9	6.3	13	37	47	25	17	1.01	1.42
3	63 (26)	13	25.1	3.6	38	60	77	49	28	0.19	0.02
4	77 (18)	13	20.0	3.2	30	39	67	29	26	0.42	0.94
5	92 (25)	14	23.7	6.9	53	58	68	54	20	0.27	1.06
6	33 (18)	9	22.3	2.0	14	42	61	20	23	0.43	1.60
7 (Figure 1)	**68 (6)**	**3**	**19.3**	**15.3**	**37**	**54**	**83**	**52**	**25**	**0.26**	**0.26**
8	172 (22)	14	25.2	5.6	73	42	55	41	28	0.10	0.82
9	77 (10)	9	18.0	1.0	45	58	90	54	27	0.01	1.79
10	184 (23)	17	24.2	17.5	94	51	74	48	29	0.92	0.92
25 August											
1	142 (30)	17	15.6	3.8	78	55	73	50	32	0.76	1.22
2	137 (9)	7	22.2	3.7	61	45	55	44	40	0.14	0.14
3	67 (24)	13	26.3	1.6	18	27	38	21	28	0.19	1.55
4 (Figure 1)	**67 (16)**	**7**	**24.6**	**2.6**	**26**	**39**	**56**	**33**	**18**	**0.48**	**0.72**
5	92 (15)	9	29.3	8.2	57	62	80	58	31	0.34	0.98
6	70 (17)	4	29.9	2.1	23	33	53	26	30	1.05	1.34
7	39 (11)	9	34.0	6.6	16	41	64	32	41	1.02	1.96
8	69 (11)	6	28.6	2.9	40	58	91	52	31	0.93	1.64
9	50 (13)	7	32.0	1.2	24	48	46	49	32	0.28	1.01
10	112 (18)	7	25.0	5.3	47	42	61	38	37	0.67	0.0
Maximum	184 (30)	17	34.0	17.5	94	62	91	58	41	1.05	1.96
Minimum	33 (6)	3	15.6	1.0	13	27	38	20	17	0.01	0.0
Average	88 (17)	10	24.6	5.5	42	47	66	41	29	0.50	1.04

Note. IB = initial breakdown; VHF = very high frequency. Column 2: Combined number of all pulses exceeding the threshold and occurring in the first 2 ms of the flash development/the number of pulses exceeding 25% of the amplitude of the largest pulse. Column 3: Number of pulses defined as "classical" IB pulses—their amplitudes exceeded 25% of the largest pulse and their duration is larger than 10 μs. Column 4: Mean duration of classical IB pulses found within the inspected period. Column 5: Mean power of VHF radiation sources calculated for VHF peaks found within the duration of classical IB pulses occurring in a given sequence. Column 6: Number of all types of IB pulses accompanied by VHF peaks within ±1 μs. Column 7: Portion of all types of IB pulses accompanied by VHF peaks within ±1 μs. Column 8: Portion of large IB pulses accompanied by VHF peaks within ±1 μs. Column 9: Portion of small IB pulses accompanied by VHF peaks within ±1 μs. Column 10: Portion of all VHF peaks above a predefined threshold accompanied by any type of IB pulses within ±1 μs. Column 11: The time of occurrence of the largest IB pulse with respect to the first recognizable IB pulse. Column 12: The time of occurrence of the largest VHF peak with respect to the first recognizable IB pulse.

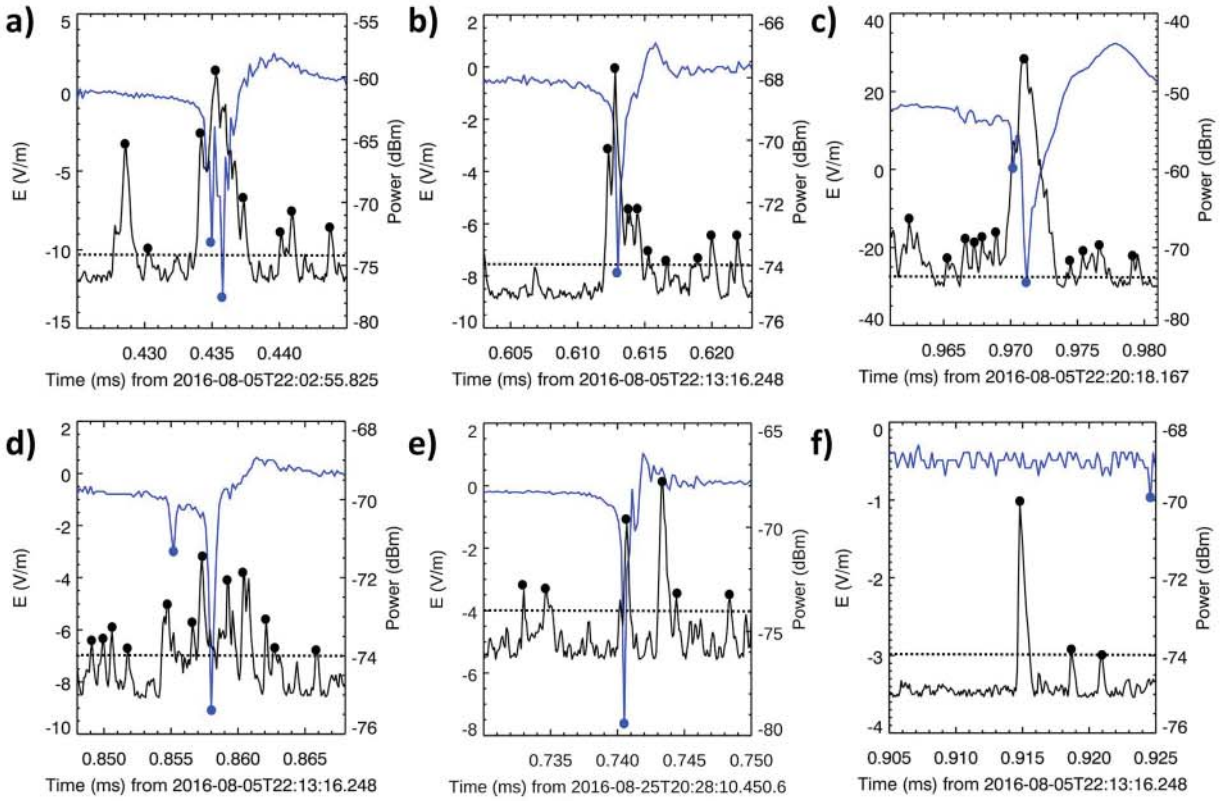

Figure 2. Examples of detailed view of Fast Antenna and LogRF data recorded at the EE station (a) and the FS station (b–d and f) on 5 August 2016. Panel (e) shows data recorded at the EE station on 25 August 2016. Black curves represent the calibrated waveforms measured by the LogRF receiver, and blue curves represent the calibrated waveforms recorded by the broadband Fast Antenna receiver. Blue and black dots identify pulse peaks chosen for our analysis. Dashed horizontal lines identify the estimates of a triple the impulsive background noise in the LogRF records.

during the leading or trailing edges of the IB pulse or during the opposite polarity overshoot. Several detailed views of IB-VHF pulse pairs are shown in Figure 2. Blue curves represent the FA measurement, and black curves represent the LogRF measurements. Dashed black lines identify the minimum power threshold of VHF pulses included in the analysis. Blue and black dots indicate which pulses were included in the basic data set. Figures 2a–2d show that there is a VHF pulse that occurred precisely matched in time (to within 1 μs) with the classical IB pulse peak. Several VHF peaks were found within the duration of the IB pulse shown in Figure 2d; the strongest VHF peak appeared between a subpulse and the main IB pulse. Two strong VHF pulses were detected within the duration of the IB pulse in Figure 2e, the weaker one was perfectly time matched with the IB peak, and the stronger pulse appeared during the opposite polarity overshoot. We have also found a substantial number of VHF pulses that were not accompanied by any FA pulse; an example of such an event is shown in Figure 2f. The precise time correspondence of all FA and VHF pulse peaks will be investigated in detail in section 4.4.

4.3. Relation of Durations of Classical IB Pulses and Powers of Corresponding VHF Pulses

The powers of sources of all VHF pulses accompanying classical IB pulses were calculated using the method described in Marshall et al. (2019). A mean power of these VHF pulses varied from 1 to 17 W within individual sequences. The power of the source of the strongest VHF pulse in the whole data set reached an exceptionally high value of 149 W, while the maximum power of sources in the other nineteen sequences varied from 2 to 44 W. A detailed view of this LogRF outlier (149 W) is shown in Figure 2c together with corresponding portion of the FA waveform. The duration of the IB pulse, which occurred simultaneously with this strongest VHF pulse, was close to the lower limit of 10 μs used for identification of classical and narrow IB pulses defined by Nag et al. (2009). The short IB pulse duration, the lack of subpulses, and the especially strong accompanying VHF radiation might indicate that this FA pulse was likely a weak low-altitude

negative narrow bipolar event occurring during the first 2 ms of the CG flash (Bandara et al., 2018; Rison et al., 2016).

In order to check for a possible relation between durations of classical IB pulses and powers of corresponding VHF pulses, we calculated Spearman rank correlation coefficients for these two properties separately for all 20 sequences. No clear correlation between durations of IB pulses and powers of corresponding VHF pulses was found. We also calculated Spearman rank correlation coefficients for the square of normalized E-field amplitude of each IB pulse divided by its duration (as a proxy for IB pulse power) and the power of the corresponding VHF pulse. We found that the random occurrence of a correlation is lower than 5% for only six sequences. Nevertheless, for all these sequences the correlation was significant, varying between 0.6 and 0.8. A few examples of the relation between durations of classical IB pulses and powers of corresponding VHF pulses are shown in the supporting information Figure S1.

4.4. Time Coincidence of IB and VHF Pulse Peaks

Section 4.2 showed the coincidence of VHF pulses occurring anytime during each classical IB pulse. In this section we examine how many of the IB pulses in the FA data are coincident with VHF pulses to within ±1 μs of the pulse peak. In looking at the two flashes shown in Figure 1, it is obvious that for each flash there are many more VHF pulses than IB pulses, and it also seems that many of the IB pulses may have coincident VHF pulses. In the flash shown in Figures 1a and 1b, there are only three classical IB pulses and all have coincident VHF pulses, as discussed above, but in addition, there are 37 IB pulses (out of 68 total) that have coincident VHF pulses within ±1 μs. Similarly, in the flash shown in Figures 1d and 1e, there are 7 classical IB pulses with coincident VHF pulses and 26 IB pulses (out of 67 total) with coincident VHF pulses within 1 μs of the peak. Thus, there are many IB pulses with coincident VHF pulses during the initiation of these two flashes. The number of time-coincident pairs varies from 13 to 94 for the 20 CG flashes. The mean value of time-coincident IB-VHF pairs per flash for the whole data set is 42. Generally, the portion of IB pulses accompanied by VHF pulses within 1 μs varies from 27% to 62% with a mean value of 47%.

Taking into account that larger and smaller IB pulses might have different properties (Nag et al., 2009), we divided all recorded IB pulses in two groups based on their amplitudes. The group with larger IB pulse amplitudes satisfied the amplitude requirement of classical IB pulses (>25% of the amplitude of the largest IB pulse in the flash), while the group of smaller IB pulses do not exceed 25% of the amplitude of the largest IB pulse. In the 20 CG flashes, the portion of larger IB pulses varies from 8% to 55% with a mean value of 24%. We find that the number of time-coincident IB-VHF pairs for the group of larger IB pulses varies from 38% to 91% with a mean value of 66%. For the group of smaller IB pulses we find generally lower portions of time-coincident IB-VHF pairs varying from 20% to 58% with a mean value of 41%. The detailed comparison of the above-mentioned characteristics is shown in the Table 1 (columns 6–10).

4.5. Relation of Amplitudes of Corresponding IB and VHF Pulse Peaks

Having identified all time-coincident IB-VHF pulse peaks occurring during the first 2 ms of the flash development, we can investigate the time evolution and possible correlation of FA and LogRF amplitudes of these IB-VHF pulse pairs. We find that generally the amplitudes of IB pulses decreases during the investigated time interval of 2 ms, but the spread of the values is very high in all cases. The amplitudes of VHF pulses as a function of time do not exhibit any trend. We did not find any clear trends in the evolution of VHF pulse amplitudes even if we excluded pulses with the smallest amplitude values from the analysis. Therefore, the trends in the time evolution of ratios of IB and VHF amplitudes also vary a lot from flash to flash and they are also dependent on the chosen threshold for removing smaller VHF pulses.

Nevertheless, when we calculate the Spearman rank correlation coefficients between both IB and VHF amplitudes and the corresponding probabilities of random occurrence of a positive or a negative correlation and take into account only 8 of the 20 flashes for which a probability of random occurrence of a correlation is lower than 5%, we have found a weak or moderate positive correlation between IB and VHF pulse amplitudes in all eight cases. The Spearman correlation coefficient for these cases varies from 0.27 to 0.51. A few examples of the relation between the amplitudes of corresponding IB and VHF pulse peaks are shown in the supporting information Figure S2.

5. Discussion

We have investigated initiation processes of 20 negative CG flashes occurring in August 2016 during two intense thunderstorms close to Oxford, Mississippi, USA. The criteria for selection of flashes included in our analysis allowed us to build a comprehensive data set, which was nevertheless sufficiently different in order to perform a reliable analysis. The detailed overview of properties of selected flashes is summarized in supporting information Table S1.

Comparison of LogRF and FA waveforms during the first 2 ms of the development of 20 investigated lightning flashes has shown that *all* identified classical IB pulses measured by FA sensors are accompanied by VHF pulses in LogRF records. Classical IB pulses have durations >10 μs, and the peaks of the accompanying VHF radiation occurred at various times during the IB pulse duration, including within ±1 μs of the IB pulse, but also near the leading edge, trailing edge or opposite polarity overshoot of the classical IB pulse. The estimated mean power of sources of VHF radiation peaks accompanying classical IB pulses was 5.5 W. These powers are several times higher than powers of LogRF events found by Marshall et al. (2019) to accompany the first classical IB pulses of two CG and two IC flashes and are about 5 orders of magnitude weaker than VHF powers of positive NBEs (detected in a frequency range of 60-66 MHz) that initiated three IC flashes (Rison et al., 2016).

Detailed investigation of the time correspondence of all pulse peaks identified in FA and LogRF records (detected at LF and VHF frequencies, respectively) that were above estimated background thresholds shows that, on average, about two thirds of IB pulses with amplitudes exceeding 25% of the amplitude of the largest IB pulse within each individual IB sequence are accompanied by VHF pulses within ±1 μs. (Note that most of these IB pulses do not have durations >10 μs.) Our results therefore indicate that electromagnetic radiation generated during fast extension of developing lightning channels is spread over a large interval of frequencies, that is, LF and VHF. We also found VHF radiation occurring in quiet periods between IB pulses; these VHF pulses might be generated by preparatory fast and small-scale corona-type discharge processes needed for the elongation of in-cloud lightning channel, as proposed by Marshall et al. (2019).

A possible correspondence of classical IB pulse durations and source powers of simultaneously appearing pulses of VHF radiation was investigated for the first time (to our best knowledge). Similarly, this is the first analysis of amplitudes of matched IB and VHF pulse peaks performed up to now. We have found that the IB pulse peak amplitudes tend to decrease within the examined 2-ms time interval. We do not see a trend in the evolution of VHF amplitudes. However, we have found a weak or moderate positive correlation between IB and VHF pulse amplitudes within eight IB sequences. We did not find any clear relation between the classical IB pulse durations and VHF source powers.

To be sure, our results are significant we checked the probability of a chance coincidence between VHF pulses and IB pulses for both the whole duration of classical IB pulses and for the ±1-μs coincidence. We have found that the probability of a ±1-μs chance coincidence varies from 0.2% to 6.0% for individual sequences with a mean value of 1.6%. The probability of a chance occurrence of VHF pulses during the minimum duration of the classical IB pulse (10 μs) varies from 0.3% to 13.9% with a mean value of 3.8%.

In conclusion, using simultaneously sampled broadband FA and narrowband LogRF waveforms we have verified the hypothesis of Kolmašová et al. (2018) that classical IB pulses are systematically accompanied by VHF radiation and that most larger-amplitude IB pulses are accompanied by VHF radiation. We have also found that the pulse amplitudes in E-change data and in LogRF data are not correlated. Our results support a hypothesis that the process of extension of in-cloud lightning leaders is very fast and highly variable. Such variations might be related to the local electrical conditions inside the thundercloud, mainly to local conductivity and distribution of charges. Our data set of 20 flashes in two storms is not sufficient for deriving general conclusions, but a further analysis of an extended data set should provide new information about the processes taking place inside thunderclouds.

Acknowledgments
The data collection was supported by NSF grants AGS-1532038 and AGS-1742930 to the University of Mississippi. I. K. thanks the Department of Physics and Astronomy of the University of Mississippi for the kind hospitality during her visits in November 2017 and 2018. The work of I. K. was supported by the Czech Academy of Sciences (MSM100421701), by European Regional Development Fund-Project CRREAT (CZ.02.1.01/0.0/0.0/15_003/0000481), and by the GACR grant 17-07027S. Processed data used to plot the figures are included in the supporting information.

References

Baharudin, Z. A., Noor, A. A., Fernando, M., Cooray, V., & Mäkelä, J. S. (2012). Comparative study on preliminary breakdown pulse trains observed in Johor, Malaysia and Florida, USA. *Atmospheric Research*, *117*, 111–121. https://doi.org/10.1016/j.atmosres.2012.01.012

Bandara, S., Marshall, T., Karunarathne, S., Karunarathne, N., Siedlecki, R., & Stolzenburg, M. (2018). Low altitude negative narrow bipolar events, paper presented at AGU Fall Annual Meeting, Abstract AE11B-2699.

Brook, M. (1992). Breakdown electric fields in winter storms. *Research Letters in Atmosphere Electronics*, *12*, 47–52.

Chapman, R., Marshall, S. K., & Stolzenburg, M. (2017). Initial electric field changes of lightning flashes in two thunderstorms. *Journal of Geophysical Research: Atmospheres*, *122*, 3718–3732. https://doi.org/10.1002/2016JD025859

Clarence, N. D., & Malan, D. J. (1957). Preliminary discharge processes in lightning flashes to ground. *Quarterly Journal of the Royal Meteorological Society*, *83*, 161–172.

Hare, B. M., Dwyer, J. R., Winner, L. H., Uman, M. A., Jordan, D. M., Kotovsky, D. A., et al. (2017). Do cosmic ray air showers initiate lightning? A statistical analysis of cosmic ray air showers and lightning mapping array data. *Journal of Geophysical Research: Atmospheres*, *122*, 8173–8186. https://doi.org/10.1002/2016JD025949

Cummer, S. A., Lyu, F., Briggs, M. S., Fitzpatrick, G., Roberts, O. J., & Dwyer, J. R. (2015). Lightning leader altitude progression in terrestrial gamma-ray flashes. *Geophysical Research Letters*, *42*, 7792–7798. https://doi.org/10.1002/2015GL065228

Karunarathne, S., Marshall, T. C., Stolzenburg, M., Karunarathna, N., Vickers, L. E., Warner, T. A., & Orville, R. E. (2013). Locating initial breakdown pulses using electric field change network. *Journal of Geophysical Research: Atmospheres*, *118*, 7129–7141. https://doi.org/10.1002/jgrd.50441

Kolmašová, I., Santolík, O., Defer, E., Rison, W., Coquillat, S., Pedeboy, S., et al. (2018). Lightning initiation: Strong VHF radiation sources accompanying preliminary breakdown pulses during lightning initiation. *Scientific Reports*, *8*(1), 3650. https://doi.org/10.1038/s41598-018-21972-z

Kolmašová, I., Santolík, O., Farges, T., Cummer, S. A., Lán, R., & Uhlíř, L. (2016). Subionospheric propagation and peak currents of preliminary breakdown pulses before negative cloud-to-ground lightning discharges. *Geophysical Research Letters*, *43*, 1382–1391. https://doi.org/10.1002/2015GL067364

Kolmašová, I., Santolík, O., Farges, T., Rison, W., Lán, R., & Uhlíř, L. (2014). Properties of the unusually short pulse sequences occurring prior to the first strokes of negative cloud-to-ground lightning flashes. *Geophysical Research Letters*, *41*, 5316–5324. https://doi.org/10.1002/2014GL060913

Kotovsky, D. A., Moore, R. C., Zhu, Y., Tran, M. D., Rakov, V. A., Pilkey, J. T., et al. (2016). Initial breakdown and fast leaders in lightning discharges producing long-lasting disturbances of the lower ionosphere. *Journal of Geophysical Research: Space Physics*, *121*, 5794–5804. https://doi.org/10.1002/2015JA022266

Lu, G., Blakeslee, R. J., Li, J., Smith, D. M., Shao, X.-M., McCaul, E. W., et al. (2010). Lightning mapping observation of a terrestrial gamma-ray flash. *Geophysical Research Letters*, *37*, L11806. https://doi.org/10.1029/2010GL043494

Marshall, T., Bandara, S., Karunarathne, N., Karunarathne, S., Kolmasova, I., Siedlecki, R., & Stolzenburg, M. (2019). A study of lightning flash initiation prior to the first initial breakdown pulse. *Atmospheric Research*, *217*, 10–23. https://doi.org/10.1016/j.atmosres.2018.10.013

Marshall, T., Karunarathne, S., Stolzenburg, M., Briggs, M., Cramer, E. S., Mailyan, B. G., et al. (2017). Electric field change measurements of a terrestrial gamma ray flash. *Journal of Geophysical Research: Atmospheres*, *122*, 5259–5266. https://doi.org/10.1002/2016JD026281

Marshall, T., Schulz, W., Karunarathna, N., Karunarathne, S., Stolzenburg, M., Vergeiner, C., & Warner, T. (2014). On the percentage of lightning flashes that begin with initial breakdown pulses. *Journal of Geophysical Research: Atmospheres*, *119*, 445–460. https://doi.org/10.1002/2013JD020854

Marshall, T., Stolzenburg, M., Karunarathna, N., & Karunarathne, S. (2014). Electromagnetic activity before initial breakdown pulses of lightning. *Journal of Geophysical Research: Atmospheres*, *119*, 12,558–12,574. https://doi.org/10.1002/2014JD022155

Marshall, T., Stolzenburg, M., Karunarathne, S., Cummer, S., Lu, G., Betz, H.-D., et al. (2013). Initial breakdown pulses in intracloud lightning flashes and their relation to terrestrial gamma ray flashes. *Journal of Geophysical Research: Atmospheres*, *118*, 10,907–10,925. https://doi.org/10.1002/jgrd.50866

Nag, A., DeCarlo, B. A., & Rakov, V. A. (2009). Analysis of microsecond- and submicrosecond-scale electric field pulses produced by cloud and ground lightning discharges. *Atmospheric Research*, *91*(2-4), 316–325. https://doi.org/10.1016/j.atmosres.2008.01.014

Rison, W., Krehbiel, P. R., Stock, M. G., Edens, H. E., Shao, X. –. M., Thomas, R. J., et al. (2016). Observations of narrow bipolar events reveal how lightning is initiated in thunderstorms. *Nature Communications*, *7*(1), 10721. https://doi.org/10.1038/ncomms10721

Smith, E. M., Marshall, T. C., Karunarathne, S., Siedlecki, R., & Stolzenburg, M. (2018). Initial breakdown pulse parameters in intracloud and cloud-to-ground lightning flashes. *Journal of Geophysical Research: Atmospheres*, *123*, 2129–2140. https://doi.org/10.1002/2017JD027729

Stolzenburg, M., Marshall, T. C., Karunarathne, S., Karunarathna, N., & Orville, R. E. (2014). Leader observations during the initial breakdown stage of a lightning flash. *Journal of Geophysical Research: Atmospheres*, *119*, 12,198–12,221. https://doi.org/10.1002/2014JD021994

Stolzenburg, M., Marshall, T. C., Karunarathne, S., Karunarathna, N., Vickers, L. E., Warner, T. A., et al. (2013). Luminosity of initial breakdown in lightning. *Journal of Geophysical Research: Atmospheres*, *118*, 2918–2937. https://doi.org/10.1002/jgrd.50276

Weidman, C. D., & Krider, E. P. (1979). The radiation field wave forms produced by intracloud lightning discharge processes. *Journal of Geophysical Research*, *84*, 159–3163.

Wilkes, R. A., Uman, M. A., Pilkey, J. T., & Jordan, D. M. (2016). Luminosity in the initial breakdown stage of cloud -to-ground and intracloud lightning. *Journal of Geophysical Research: Atmospheres*, *121*, 1236–1247. https://doi.org/10.1002/2015JD024137

Wu, T., Takayanagi, Y., Funaki, T., Yoshida, S., Ushio, T., Kawasaki, Z.-I., et al. (2013). Preliminary breakdown pulses of cloud-to-ground lightning in winter thunderstorms in Japan. *Journal of Atmospheric and Solar - Terrestrial Physics*, *102*, 91–98. https://doi.org/10.1016/j.jastp.2013.05.014